13th EWTEC 2019
Proceedings of the 13th European Wave and Tidal Energy Conference 1-6 Sept 2019, Naples, Italy

Metrics for wave energy converter hull geometry optimisation

Anna Garcia-Teruel, David I. M. Forehand, and Henry Jeffrey

***Abstract*—Wave Energy Converter (WEC) structures have been widely studied in the past decade, due to their high potential for device cost reduction. In this context, various hull geometry optimisation studies have been performed to maximise power and reduce costs, where costs were mostly represented through the device size in terms of mass, volume or surface area. In the present study, the suitability of the different objective functions is analysed, with the goal of finding an optimal hull shape with relevant cost considerations when using a flexible geometry definition. The results are given for a particular location off the West Shetland shelf to the north of Scotland. Impedance matching control at the energy period is assumed, and this means that mass distribution has no effect on the device oscillation. The differences in shape and annual energy production are presented for optimal devices oscillating in surge, and in surge, heave and pitch. Devices are optimised for maximal annual energy production, and its ratio to various size characteristics based on volume and surface area.**

***Index Terms*—Hull geometry, Optimisation, Wave energy converters**

I. Introduction

TO find an economically competitive design of a Wave Energy Converter (WEC), device geometry has been optimised in previous studies not only for performance maximisation, but also for cost minimisation - with the cost usually represented by the device's size [1]–[4]. However, resulting shapes can be inadequate to survive in high energetic seas or not cost-effective to manufacture. Additionally, these studies were restricted to the analysis of devices with predefined shapes of variable dimensions or pre-specified modes of oscillation. Some of these limitations were overcome by using a flexible geometry definition, as in McCabe [5], and by expanding the analysis to assess different factors related to the device's geometry that can have an effect on costs [6]. However, it has been found that the volume is not always a good proxy for costs in the objective function of a geometry optimisation process [7]. In [7], Garcia-Teruel et al. found that shapes optimised using volume as the cost proxy resulted in complex shapes with increased surface area perpendicular to the energy extracting direction. These shapes would probably require complex manufacturing processes and large amounts of material. With a similar reasoning, Driscoll et al. [8] proposed representing structural costs through the device surface area and a representative hull thickness for the Wave Energy Prize. As a result, the present study investigates the suitability of different metrics for cost representation in the objective function. This will then affect the optimal device shape.

This study is performed for a point absorber with a single-objective optimisation approach, based on a frequency-domain hydrodynamic model, together with a genetic algorithm for geometry generation and selection, as used in [5]. In that previous study, each WEC geometry was defined by a set of variable control points and an initial population of WEC shapes was created by varying these points randomly. By means of algorithms defining selection, recombination and mutation processes, as they are known from evolution theory, geometries which best fulfil the defined requirements were used to create further generations of WECs. After a number of iterations (generations), it was hoped that the genetic algorithm would converge on an optimal WEC shape. The objective functions used in that optimisation method were the maximal power extraction, the ratio of maximal power extraction to the cube root of the displaced volume and the ratio of maximal power extraction to the displaced volume. However, as mentioned previously, resulting shapes were very complex; difficult to manufacture; and had large surface areas; and, thus, increased costs. The aim of this study is, therefore, to substitute the cost proxies based on the device's submerged volume with cost proxies based on its actual submerged surface area. This is expected to generate more realistic solutions since structural costs will be directly related to the amount of material required, which is represented by the surface area and the wall thickness of the device. These will be compared with results obtained using the objective functions of the original study with the aim of finding the most suitable representation of costs for this particular application.

II. Methodology

A. Optimisation process

The re-implemented geometry optimisation process follows the approach of McCabe in [5]. A flow diagram of the process is represented in Fig. 1. An overview of this process is given here, but note that it has been previously described in [7] with further detail.

Submission ID 1585, Track: WHM. This work was supported through funding from the University of Edinburgh, Energy Technology Partnership and SuperGen Marine.

A. Garcia-Teruel is at the Institute for Energy Systems at the University of Edinburgh, The King's Buildings, Max Born Crescent, EH9 3BF Edinburgh, United Kingdom (a.garcia-teruel@ed.ac.uk).

D. Forehand is at the Institute for Energy Systems at the University of Edinburgh, The King's Buildings, Max Born Crescent, EH9 3BF Edinburgh, United Kingdom (d.forehand@ed.ac.uk).

H. Jeffrey is at the Institute for Energy Systems at the University of Edinburgh, The King's Buildings, Max Born Crescent, EH9 3BF Edinburgh, United Kingdom (henry.jeffrey@ed.ac.uk).

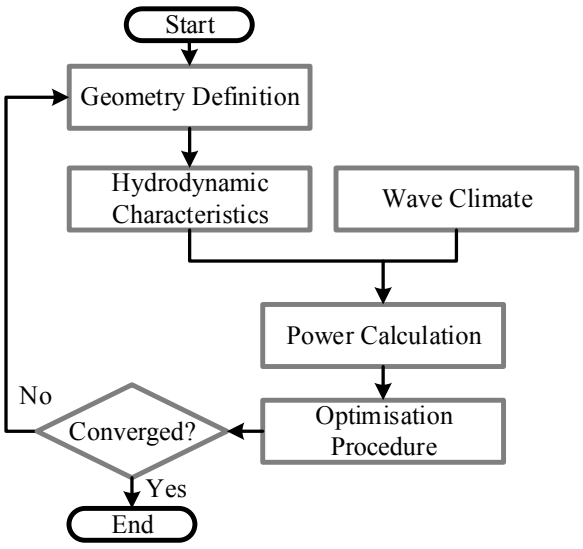

Fig. 1. Flow diagram of the WEC geometry optimisation process.

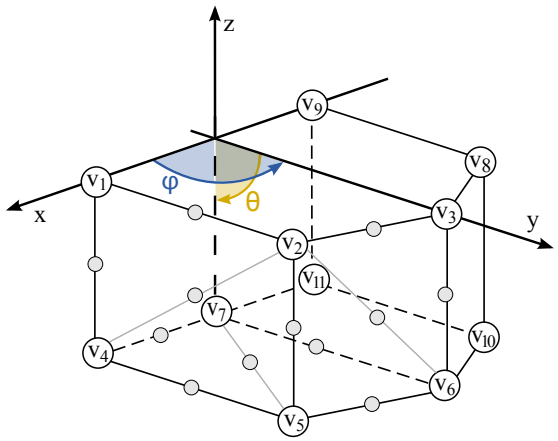

Fig. 2. Schematic representation of the polyhedron vertices for the geometry definition, some examples of interpolated points are shown in gray.

The geometry is defined so that resulting shapes can take many different forms in a way which is as free from human intervension as possible. This process is explained in section II-B. The shapes are then assessed based on their performance. Their hydrodynamic characteristics are obtained by employing the commercial radiation/diffraction code WAMIT [9] and their power performance is evaluated with a frequency domain model introduced in section II-C. The genetic algorithm used to generate new geometries from the better-performing ones is described in section II-D.

B. Geometry definition

The geometry is defined with help of the corner points of a polyhedron with an x-z-symmetry plane (see Fig. 2). Following McCabe's preferred interpolation method [10] further points are interpolated between the corner points. They all serve as control points to build a bi-cubic B-spline surface, which is a smooth surface that approximates the points without necessarily going through them. The control points can move randomly in space within the defined limits. Considering that some of the coordinates of the control points are fixed, such as for points lying on the free surface or on the symmetry plane, 22 coordinates are variable. These constitute the optimisation variables $(v_1, v_2, ..., v_{22})$ of this optimisation problem.

C. Hydrodynamic model

The annual energy production of each geometry at a location on the West-Shetland shelf is used to represent the device's performance. For the wave energy resource, irregular unidirectional waves in a fully developed sea represented by a Bretschneider spectrum are employed. The occurrence matrix for this location is reported in [5]. The hydrodynamic characteristics for each shape are calculated in WAMIT based on the frequencies selected to represent the spectrum, which are the 150 frequencies (ω_k) from 0 to 3 rad/s in 0.02 rad/s steps. The hydrodynamic model is based on the assumption that linear wave theory can be applied, and that the device oscillations are small. This means that the device motions can be described as the superposition of multiple harmonic oscillations.

In this case, the oscillatory response in six degrees of freedom of a WEC can be described using the complex amplitude of oscillation $\hat{\mathbf{X}}(\omega_k)$, as in (1).

$$\begin{aligned}\hat{\mathbf{X}}(\omega_k) = [\mathbf{K} - \omega_k^2(\mathbf{M} + \mathbf{M}_a(\omega_k)) + \\ i\omega_k(\mathbf{C}_a(\omega_k) + \mathbf{C}_{loss})]^{-1}\hat{\mathbf{F}}_e(\omega_k)\alpha(\omega_k) \\ \text{with} \quad \alpha(\omega_k) = \sqrt{(2S(\omega_k)\Delta\omega)}\end{aligned} \tag{1}$$

The main forces involved in this oscillation are considered here as in a mass-spring-damper-system through the following terms: the hydrostatic stiffness matrix $\mathbf{K}$, the mass matrix of the device $\mathbf{M}$, the radiation terms: added mass $\mathbf{M}_a(\omega_k)$ and added damping $\mathbf{C}_a(\omega_k)$ matrices, the complex amplitude of the excitation force vector $\hat{\mathbf{F}}_e(\omega_k)$ and an additional damping matrix $\mathbf{C}_{loss}$ to account for friction losses, as in [5]. The excitation force vector is normalised for a 1 meter wave amplitude. For this reason, the oscillation needs to be scaled by the wave amplitude for each frequency component $\alpha(\omega_k)$.

If assuming the idealised optimal impedance matching control at the energy period $T_e = 2\pi/\omega_e$, as introduced by Falnes in [11] and implemented for the Pelamis device in [12], the mass $\mathbf{M}$ and stiffness $\mathbf{K}$ terms can be cancelled from the equation of motion (2), so that this becomes independent of the mass distribution.

$$\begin{aligned}\hat{\mathbf{X}}(\omega_k) = &[\omega_k^2(\mathbf{M}_a(\omega_k) - \mathbf{M}_a(\omega_e)) + \\ &i\omega_k(\mathbf{C}_a(\omega_k) + \mathbf{C}_a(\omega_e) + 2\mathbf{C}_{loss})]^{-1}\hat{\mathbf{F}}_e(\omega_k)\alpha(\omega_k)\end{aligned} \tag{2}$$

The instantaneous power available at the Power Take-Off (PTO) system, is calculated from the power absorbing terms of the PTO force and the oscillation velocity $\dot{\mathbf{x}}_q(t)$ in (3).

$$P_{U,q}(t) = \dot{\mathbf{x}}_q^T(t)[\mathbf{C}_a(\omega_e) + \mathbf{C}_{loss}]\dot{\mathbf{x}}_q(t) \tag{3}$$

Applying this as a time series allows the limitation of the maximal allowable PTO stroke in the six modes

of motion i=1,...,6 and its power rating. The time series for the oscillation velocity is obtained from the oscillation time series through derivation. The latter is composed of the superposed harmonic oscillations of different amplitudes and frequencies. Each oscillation of frequency k is assigned a random phase shift $\psi_{k,q}$ from a set of random phase shifts $q = 1, ..., 10$.

$$x_{i,q}(t) = \sum_{k=1}^{N} \Big(\big|X_i(\omega_k)\big| \cos(\omega_k t + \psi_{k,q} + \angle X_i(\omega_k)) \Big) \quad (4)$$

The instantaneous power $P_{U,q}(t)$ is integrated over time t and averaged over the time period and the sets of random phase shifts q, so that a mean power per sea state $\bar{\mathbf{P}}(H_{m0}, T_z)$ is obtained. Combining this with the sea states occurrence matrix $\mathbf{O}(H_{m0}, T_z)$, results in the annual average power $\bar{P}$.

$$\bar{P} = 1/8760 \sum_{H_{m0}} \sum_{T_z} [\mathbf{O}(H_{m0}, T_z) \times \bar{\mathbf{P}}(H_{m0}, T_z)] \quad (5)$$

The annual average power and the displaced volume V are employed in the objective functions of the original implementation [5], where the volume's cubic root is used as a proxy for a characteristic length. The following objective functions are minimised in the optimisation process.

$$f_1 = -\bar{P} = f(v_1, v_2, ..., v_{22}) \quad (6)$$

$$f_2 = -\frac{\bar{P}}{V} = f(v_1, v_2, ..., v_{22}) \quad (7)$$

$$f_3 = -\frac{\bar{P}}{\sqrt[3]{V}} = f(v_1, v_2, ..., v_{22}) \quad (8)$$

The newly introduced objective functions are based on the actual submerged surface area S, where its square root is also used as proxy for a characteristic length, and the displaced volume exponentiated to $2/3$ is used as a proxy for the submerged surface area. These objective functions are also set to be minimised within the optimisation process.

$$f_4 = -\frac{\bar{P}}{V^{2/3}} = f(v_1, v_2, ..., v_{22}) \quad (9)$$

$$f_5 = -\frac{\bar{P}}{S} = f(v_1, v_2, ..., v_{22}) \quad (10)$$

$$f_6 = -\frac{\bar{P}}{\sqrt{S}} = f(v_1, v_2, ..., v_{22}) \quad (11)$$

D. Geometric characteristics

The displaced volume V can be obtained from WAMIT for each geometry. To calculate the submerged surface area S various methods were employed to compare their accuracy versus the required computation time. The submerged surface area is calculated through discretisation of the parametric surface (Method I), as the sum of the areas of all the triangles making up the surface. Triangles are used instead of quadrilaterals, given that the points on the surface are not coplanar, and that the projection of the points on a common plane would be required. The same method is applied using the low-order mesh outputted from WAMIT rather than the discretised parametric surface (Method II). Both these methods were compared to the results from the integral of the parametric surface function (Method III). The calculation time for Method III was 851s on average per geometry. For Method I the surface area calculation time varied from 4.77s to 664.46s, depending on the resolution of the discretisation, with an average percentage difference from the reference area from -0.129 to -0.003%. For Method II, analogously, depending on the chosen resolution the additional calculation time varied from 2.06s to 20.03s for an average percentage difference from the reference surface area ranging from 0.07 to 0.05%. For this reason, Method II with the lower resolution was used. This is equivalent to setting ILOWGDF=20 in WAMIT. The difference in calculation time is, therefore, of approxximately 2.06s more per geometry than if using the submerged volume.

E. Optimisation algorithm

A single-objective genetic algorithm is employed based on the University of Sheffield's implementation [13]. 22 randomly generated geometries form the initial population, out of which 10 are selected through Stochastic Universal Sampling to pair by Intermediate Recombination [14]. In this way 20 new individuals are created. Each of these new individuals will undergo on average 3 mutations over the number of variables (22) so that new characteristics that were not present in the parent generation are introduced. To ensure that the genetic material of the best performing individuals is kept in the new generation, Elite Reinsertion is used, where the two best performing individuals are kept in the population. The 20 newly generated individuals and the 2 best parents form the new generation of the same size as the previous one. This process is iterated over 100 generations, or after a minimum of 50 generations, if the objective function does not improve over 20 generations, the algorithm is considered to have converged.

III. Results

The resulting optimal shapes shown in Fig. 3 are compared based on their performance, volume and surface area. The corresponding objective function values for the surging only case can be found in Table I and for the surging, heaving, and pitching case in Table II. These preliminary results show indicative trends, however, the obtained solutions might be suboptimal, since the employed optimisation algorithm might not be the most suitable for all cases. In general, population-based metaheuristic optimisation algorithms such as genetic algorithms, are suitable for finding good solutions to complex problems. However, other algorithms exist with similar charactertics but with different approaches for the exploration and exploitation of the solution space (e.g. the Particle Swarm Optimization method). Additionally, all of the above algorithms have various settings that need to be tuned

to the investigated problem (such as the number of individuals in the population, the number of pairings or the mutation rate). The choice of the objective function also changes the shape of the solution space, and therefore, changes the most suitable strategy to navigate it. The appropriateness of the applied optimisation algorithm for the different objective functions is the subject of a further study.

TABLE I
OVERVIEW OF THE OPTIMISATION RESULTS FOR A DEVICE OSCILLATING IN SURGE

Objective Function	Power [kW]	Volume [m^3]	Surface area [m^2]
$f_1 = \bar{P}$	357,541.995	3,464.463	895.698
$f_2 = \frac{\bar{P}}{V}$	144,617.825	250.060	332.727
$f_3 = \frac{\bar{P}}{\sqrt[3]{V}}$	216,288.125	333.472	494.231
$f_4 = \frac{\bar{P}}{V^{2/3}}$	183,818.684	250.985	436.969
$f_5 = \frac{\bar{P}}{S}$	205,661.877	930.560	401.445
$f_6 = \frac{\bar{P}}{\sqrt{S}}$	277,876.036	1,616.067	574.929

TABLE II
OVERVIEW OF THE OPTIMISATION RESULTS FOR A DEVICE OSCILLATING IN SURGE, HEAVE AND PITCH

Objective Function	Power [kW]	Volume [m^3]	Surface area [m^2]
$f_1 = \bar{P}$	949,898.242	2,366.713	799.060
$f_2 = \frac{\bar{P}}{V}$	643,150.376	250.317	287.376
$f_3 = \frac{\bar{P}}{\sqrt[3]{V}}$	807,358.697	388.751	579.619
$f_4 = \frac{\bar{P}}{V^{2/3}}$	656,519.842	250.089	307.027
$f_5 = \frac{\bar{P}}{S}$	503,173.851	250.257	182.852
$f_6 = \frac{\bar{P}}{\sqrt{S}}$	277,876.036	1,616.067	574.929

In both cases, geometries optimised to maximise power (f_1) do indeed generate the highest annual average power of up to 85% more than the lowest power generation values achieved in surge by f_2 and up to 60% in surge, heave, and pitch by f_6. Regarding the volume and surface area, the highest values are achieved, as expected, by geometries optimised to maximise power only since costs are not penalised in any way. In contrast, the lowest volume values are very similar in both cases for f_2 and f_4 tending towards the minimum set limit for the displaced volume of 250m^3. For a device oscillating in surge, heave, and pitch, this is also the case for geometries optimised for f_5. Interestingly, although generally lower surface area values are achieved when using f_5 and f_6, in the surge only case the lowest surface area value is achieved by f_2, with which a relatively low value can also be observed in the multi-modal case.

When looking at the $\frac{\bar{P}}{V}$ and $\frac{\bar{P}}{S}$ ratios, as represented in Table III, it is interesting to see that the results obtained for $\frac{\bar{P}}{V}$ from f_4 are better than for f_2. This points to the fact that the optimisation algorithm employed in this study might work better for the objective function f_4 than for f_2. For this reason, a detailed study of the optimisation algorithm suitability is required. Despite the low surface areas being achieved by f_2, the ratio of $\frac{\bar{P}}{S}$ is best for geometries optimised with f_5 as expected.

TABLE III
OVERVIEW OF THE OPTIMISATION RESULTS FOR A DEVICE OSCILLATING IN SURGE

Objective Function	Surge		Surge, Heave and Pitch	
	$\frac{\bar{P}}{V}$ [kW/m^3]	$\frac{\bar{P}}{S}$ [kW/m^2]	$\frac{\bar{P}}{V}$ [kW/m^3]	$\frac{\bar{P}}{S}$ [kW/m^2]
$f_1 = \bar{P}$	103.203	399.177	401.358	1,188.770
$f_2 = \frac{\bar{P}}{V}$	578.332	434.644	2,569.344	2,238.010
$f_3 = \frac{\bar{P}}{\sqrt[3]{V}}$	648.595	437.626	2,076.802	1,392.913
$f_4 = \frac{\bar{P}}{V^{2/3}}$	736.389	420.668	2,625.145	2,138.313
$f_5 = \frac{\bar{P}}{S}$	221.009	512.304	2,010.628	2,751.809
$f_6 = \frac{\bar{P}}{\sqrt{S}}$	171.946	483.322	2,455.058	2,433.454

Regarding the resulting shapes (see Fig. 3), it becomes apparent that shapes optimised based on volume cost proxies tend to have higher curvatures and thinner cross-sections, whereas shapes optimised based on surface area cost proxies tend to be smoother. From a manufacturing and structural integrity perspective, lower curvature, smooth structures of bigger cross-section will have a more even stress distribution. This will also allow for internal structural reinforcement and easier manufacturing, and will, therefore, be more cost efficient. Note, for each of the subfigures (a) to (l) in Fig. 3, there are two images of the corresponding optimal submerged geometry. The left image is a view of the geometry from above the free surface and the right image is a view from below the free surface.

With regards to the computation time, the average run time for a 1 degree-of-freedom optimisation was approximately 21h on an i7 Optiplex 9010 computer with 32GB of RAM. For the multiple degrees-of-freedom case, this increased to approximately 37h. In the case of using the submerged surface area instead of the submerged volume, for 100 generations over which 20 new individuals were evaluated per generation, the additional required run time was 4124.12s (approximately 1.15h) more per optimisation run. The authors consider this 3-5% increase of the total computational time to be reasonable. However, it must be noted that the total run time depends highly on the available computation resources.

IV. CONCLUSION

Different objective functions for geometry optimisation of WECs have been compared, based on results obtained using genetic algorithms and a flexible geometry definition. The results show that although using volume in different ways as a proxy for costs,

leads to optimal shapes with lower volume and surface area, shapes optimised based on surface area proxies result in smoother structures with bigger cross-section. These latter shapes will also have manufacturing and structural integrity advantages. From the compared metrics it seems like f_5 is the most suitable objective function for geometry optimisation of WECs since it results in both lower surface area and lower volumes than f_6. However, f_6 shows higher power production values. For further comparison, a multi-objective study of a WEC hull geometry optimised for both power and surface area simultaneously, would be beneficial. This would give further insight into the effect that surface area has on the resulting optimal shapes, depending on the relative importance of each of the objectives.

Furthermore, the suitability of the optimisation algorithm can change with the use of different objective functions. For this reason, this should be examined further, to ensure a fair comparison of the objective functions.

REFERENCES

[1] R. Gomes, J. C. C. Henriques, L. M. C. Gato, and A. F. O. Falcão, "IPS Two-body Wave Energy Converter : Acceleration Tube Optimization," in *Isope*, vol. 7, no. 4, 2010, pp. 834–842.

[2] J.-C. Gilloteaux and J. Ringwood, "Control-informed geometric optimisation of wave energy converters," *IFAC Proceedings Volumes*, vol. 43, no. 20, pp. 366–371, sep 2010. [Online]. Available: https://www.sciencedirect.com/science/article/pii/S1474667016334905

[3] A. Kurniawan and T. Moan, "Multi-objective optimization of a wave energy absorber geometry," *27th International Workshop on Water Waves and Floating Bodies*, no. 2, pp. 3–6, 2012.

[4] M. Blanco, M. Lafoz, and G. Navarro, "Wave energy converter dimensioning constrained by location, power take-off and control strategy," in *2012 IEEE International Symposium on Industrial Electronics*. IEEE, may 2012, pp. 1462–1467. [Online]. Available: http://ieeexplore.ieee.org/document/6237307/

[5] A. McCabe, "Constrained optimization of the shape of a wave energy collector by genetic algorithm," *Renewable Energy*, vol. 51, pp. 274–284, mar 2013. [Online]. Available: http://www.sciencedirect.com/science/article/pii/S0960148112006258

[6] A. Garcia-Teruel, D. I. Forehand, and H. Jeffrey, "Wave Energy Converter hull design for manufacturability and reduced LCOE," *Icoe 2018*, pp. 1–9, 2018. [Online]. Available: https://www.icoe-conference.com/publication/wave-energy-converter-hull-design-for-manufacturability-and-reduced-lcoe/

[7] A. Garcia-Teruel and D. Forehand, "Optimal wave energy converter geometry for different modes of motion," in *Advances in Renewable Energies Offshore: Proceedings of the 3rd International Conference on Renewable Energies Offshore (RENEW 2018)*, Lisbon, 2018, pp. 299–305.

[8] F. Driscoll, J. Weber, S. Jenne, R. Thresher, L. J. Fingersh, D. Bull, A. Dallman, B. Gunawan, A. Labonte, D. Karwat, S. Beatty, F. Driscoll, J. Weber, R. Thresher, L. Jay, D. Bull, A. Dallman, B. Gunawan, and S. Beatty, "Methodology to Calculate the ACE and HPQ Metrics Used in the Wave Energy Prize," no. March 2018, 2018.

[9] MIT, "WAMIT User Manual." [Online]. Available: http://www.wamit.com/manualupdate/V70_manual.pdf

[10] A. P. McCabe, G. A. Aggidis, and M. B. Widden, "Optimizing the shape of a surge-and-pitch wave energy collector using a genetic algorithm," *Renewable Energy*, vol. 35, no. 12, pp. 2767–2775, 2010. [Online]. Available: http://dx.doi.org/10.1016/j.renene.2010.04.029

[11] J. Falnes, *Ocean Waves and Oscillating Systems*. New York: Cambridge University Press, 2002.

[12] R. Henderson, "Design, simulation, and testing of a novel hydraulic power take-off system for the Pelamis wave energy converter," *Renewable Energy*, vol. 31, no. 2, pp. 271–283, feb 2006. [Online]. Available: https://www.sciencedirect.com/science/article/pii/S0960148105002259

[13] A. Chipperfield, P. Fleming, H. Pohlheim, and C. Fonseca, "Genetic Algorithm Toolbox - User's Guide," 1995. [Online]. Available: http://codem.group.shef.ac.uk/public/GAToolbox_Documentation.pdf

[14] H. Mühlenbein and D. Schlierkamp-Voosen, "Predictive Models for the Breeder Genetic Algorithm," *Evolutionary Computation*, vol. 1, no. 1, pp. 25–49, 1993. [Online]. Available: http://citeseerx.ist.psu.edu/viewdoc/download?doi=10.1.1.74.9357&rep=rep1&type=pdf

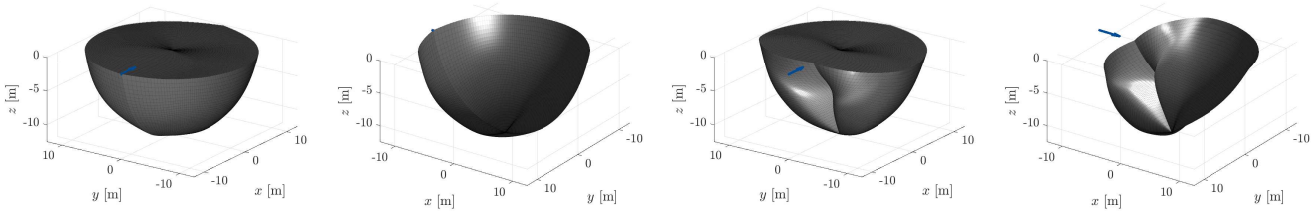

(a) P, Surge

(b) P, Surge, Heave and Pitch

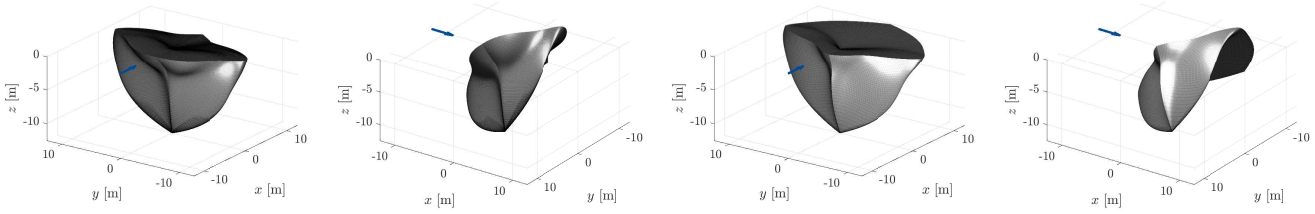

(c) $\frac{\bar{P}}{\sqrt[3]{V}}$, Surge

(d) $\frac{\bar{P}}{\sqrt[3]{V}}$, Surge, Heave and Pitch

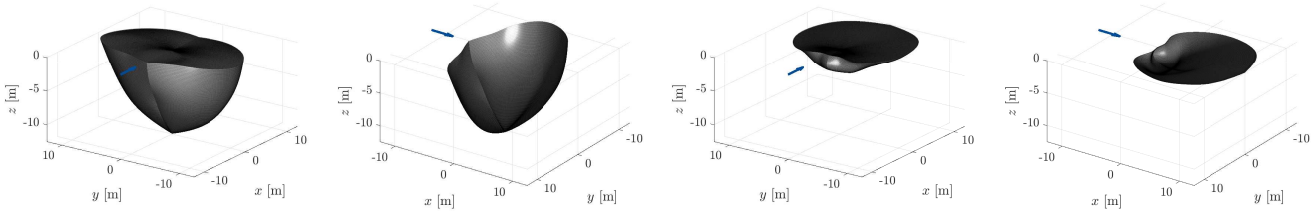

(e) $\frac{\bar{P}}{\sqrt{S}}$, Surge

(f) $\frac{\bar{P}}{\sqrt{S}}$, Surge, Heave and Pitch

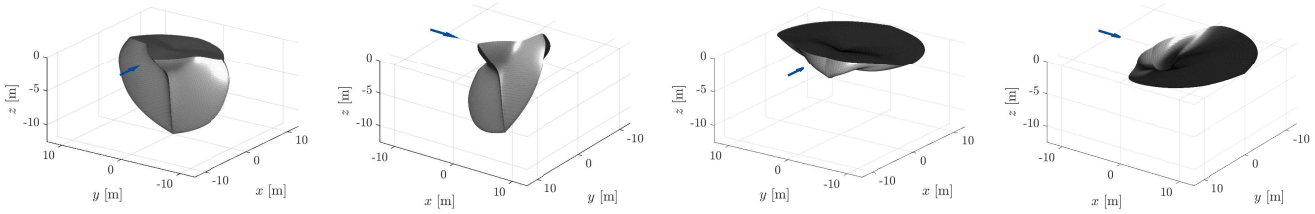

(g) $\frac{\bar{P}}{V^{2/3}}$, Surge

(h) $\frac{\bar{P}}{V^{2/3}}$, Surge, Heave and Pitch

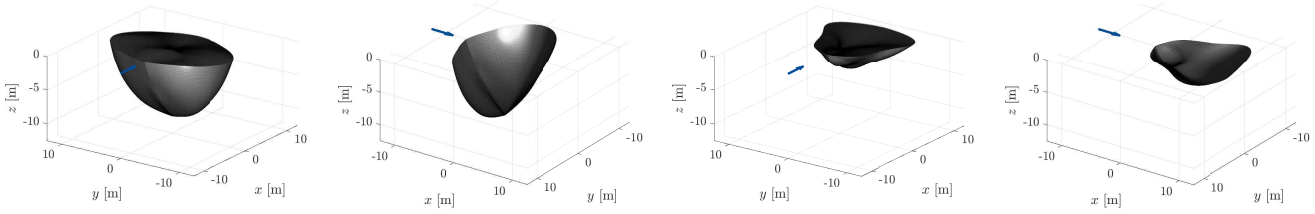

(i) $\frac{\bar{P}}{S}$, Surge

(j) $\frac{\bar{P}}{S}$, Surge, Heave and Pitch

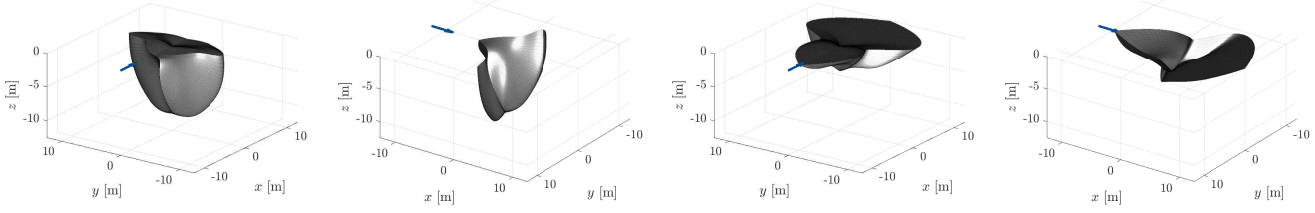

(k) $\frac{\bar{P}}{V}$, Surge

(l) $\frac{\bar{P}}{V}$, Surge, Heave and Pitch

Fig. 3. Resulting optimal geometries for WECs oscillating in surge only (left two columns) and in surge, heave and pitch (right two columns) and optimised for six objective functions.